ACS Chemical Biology
pubs.acs.org/acschemicalbiology
Article

Quantitative Degradation Rate Assessment of bioPROTACs Based on Peptide Degrons, E3 Domains, Adapters and Conjugated Small Molecules

David Vukovic,[§] Dorothea Winkelvoß,[§] Anto Udovcic, Luca Riermeier, Saul Jaime-Figueroa, Craig M. Crews, and Andreas Plückthun*

Cite This: https://doi.org/10.1021/acschembio.5c00569
Read Online

ABSTRACT: Protein-based bispecific degraders, known as bioPROTACs, have emerged as powerful tools for targeted protein degradation through the ubiquitin-proteasome system (UPS). However, the relative efficacy of various recruitment domains within these degraders remains poorly understood. To address this knowledge gap, we conducted a comprehensive comparison of recruitment domains in bioPROTACs, utilizing eGFP as a proof-of-principle degradation target and an eGFP-binding DARPin with known structure as an adapter. Our innovative approach combined microinjection and live-cell microscopy, enabling a detailed assessment of directly measured degradation rates as a single-cell kinetic readout, unaffected by uptake or biosynthesis rates of the degrader, and across the different chemical classes. We examined nine degron peptides, three E3 ligase domains or adapters, and two series of small-molecule binders, linked in various geometries. Our results revealed that bioPROTACs based on E3 or adapter protein domains and small molecules generally exhibited the highest degradation rates, while most degron peptides showed comparatively low efficacy. Notably, for VHL-ligand-1 and thalidomide, the placement of the coupling site and linker position significantly influenced performance. This study provides crucial insights into the design and optimization of bioPROTACs, paving the way for the development of more effective degraders for specific applications. Our findings contribute to the growing field of targeted protein degradation and offer valuable guidance for researchers seeking to enhance the efficacy of bioPROTAC-based therapeutic approaches.

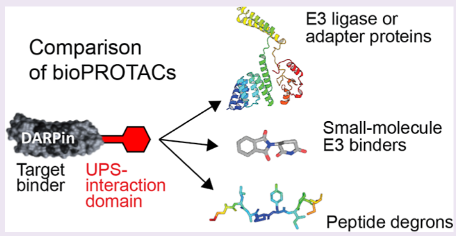

INTRODUCTION

The human proteome undergoes constant synthesis and degradation, with selective protein degradation playing a pivotal role in numerous cellular processes.[1] These include cell cycle progression, signal transduction, development, differentiation, transcriptional regulation, antigen presentation, receptor-mediated endocytosis, quality control, and modulation of various metabolic pathways.[2] In eukaryotes, the ubiquitin proteasome system (UPS) primarily orchestrates regulated protein degradation of intracellular proteins.[3] Consequently, the UPS system has also become a platform for drug targeting.[4] A novel therapeutic approach harnesses the UPS for the enzymatic degradation of dysfunctional or overexpressed proteins using bispecific small molecules known as proteolysis-targeting chimeras (PROTACs).[5] These molecules concurrently engage a specific protein target and an E3 ligase, facilitating target ubiquitination and subsequent proteasomal degradation (Figure 1a).

This mode of action offers several advantages over traditional small-molecule inhibitors due to its catalytic nature, including potentially lower dosage requirements and sustained responses.[5] However, within the realm of PROTAC research, the scarcity of available warheads to target E3 ligases poses a challenge.[6] Likewise, small-molecule binders for specific targets are often lacking, particularly for proteins devoid of natural small molecule-binding pockets, and this renders a significant portion of the proteome ″undruggable″. Factors involved in epigenetic modifications have been recognized as excellent targets, as they typically do have binding pockets for cofactors, e.g. for methylation.[7] On the other hand, other proteins at pivotal points of transcriptional regulation, such as many transcription factors, do not have suitable binding pockets for small molecules.

To address this problem, protein binders have been investigated for the design of bioPROTACs.[8] A number of different peptides, natural proteins and engineered binding proteins have been tested as target-interaction domains in bioPROTACS, yet usually only in semiquantitative experiments and not in direct comparisons aiming to elucidate the factors leading to efficient degradation.[9−17] While small-

Received: July 23, 2025
Revised: November 22, 2025
Accepted: November 24, 2025

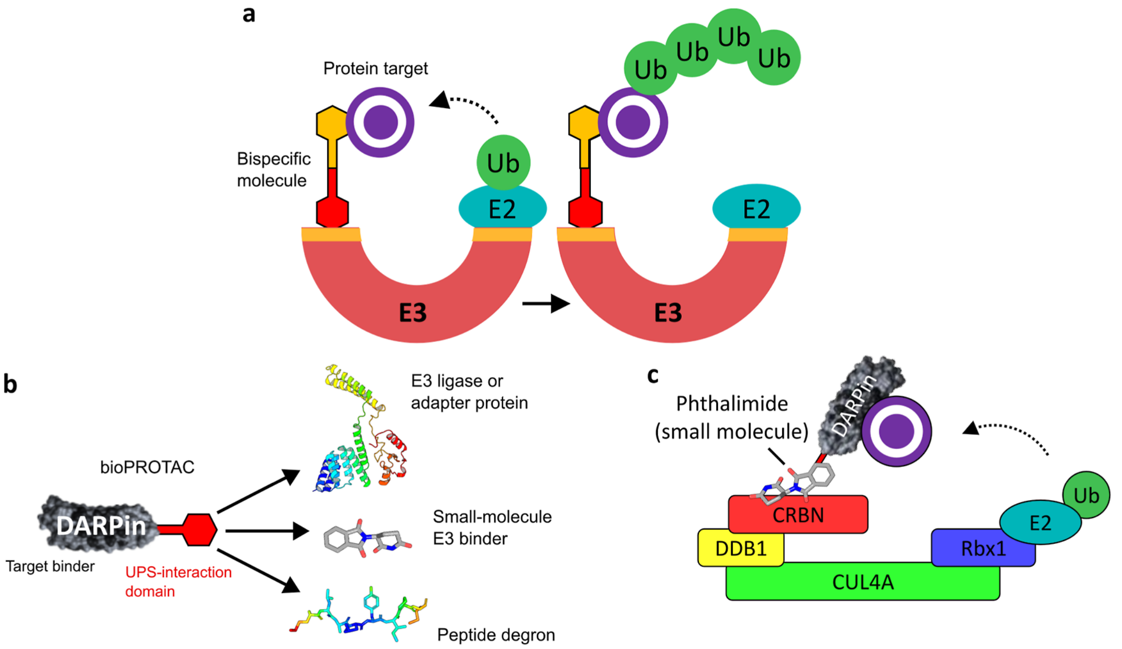

Figure 1. BioPROTAC design for targeted protein degradation. (a) Principle of bispecific degraders. (b) Design strategies for UPS interaction domain of bioPROTACs. (Examples: CHIP E3 ligase, PDB ID: 2C2L (top); Thalidomide, PDB ID: 4V32 (middle); MLAPYIPM degron from HIF1α, PDB ID: 1LM8 (bottom)). (c) Example of small-molecule-based bioPROTAC working principle.

molecule PROTACs have often been meticulously designed considering different linkers, geometries and optimization of binding moieties for the target and the E3 ligase, detailed design principles for bioPROTACs remain relatively scarcely studied in a systematic fashion. We previously elucidated design principles for the target binding domain of bioPROTACs, and we concentrated there on defining the optimal properties of target-binding moiety of bioPROTACs.[18]

Briefly, we found that the geometry of interaction is very critical, while affinity and stability play only a minor role.[18] In that study, we used the very efficient UPS interaction domain from CHIP E3 ligase, and 9 different well-characterized DARPins to test degradation of the proof-of-principle target eGFP. All but two DARPins work well in this context, one sterically preventing E2 binding in the complex, the other overlapping with the target ubiquitination epitope. BioPROTACs constructed in this way were able to degrade eGFP catalytically.

As a control, we had also established that DARPins by themselves could also accelerate degradation of bound GFP, engaging other cellular E3 systems, but in a noncatalytic manner.[18] The most important factor for efficient degradation by a bioPROTAC in trans is the correct orientation of the complex for target ubiquitination and presentation to the proteasome, which still needs to be determined empirically.

In the previous study,[18] we had compared the efficiency of various GFP-binding DARPins with a same UPS interaction domain from CHIP E3 ligase. In the present study, we aimed for a complementary approach to explore and compare different strategies for UPS interaction in conjunction with the same target-binding DARPin (Figure 1b). These strategies included peptide degrons recognized by a specific E3 ligase, complete E3 ligases, adapter proteins for an E3 ligase complex, and small-molecule E3 binders. We selected several previously reported as well as novel E3 domains, along with well-known small-molecule binders such as thalidomide and VHL-ligand-1, which are currently employed in PROTACs undergoing clinical trials.[19] Building on the well-established influence of linker length on the efficacy of small-molecule PROTACs, we also investigated the impact of varying linker lengths and coupling positions within the DARPin for the design of small-molecule-based bioPROTACs. While the linker may also influence the degradation efficiency of bioPROTACS, we have not varied them in the present study as the fusion arrangement has been mostly taken from natural systems.

Comparing these very different substance classes (E3 ligase domains, degron peptides, small molecule PROTACS) is challenging at several levels. First, we have to engage the same target, independent of any present small-molecule binding site. For this reason, we chose the model target eGFP with an N-terminal extension of two amino acids (Gly−Ser), termed GS-eGFP. We had shown previously that this extension is necessary and sufficient[18,20] to bring GFP to degradation in a time range that can be conveniently observed by fluorescence decrease with semiautomatic microscopy. Second, we have to use the same binding module to bring degradation domains in proximity and be able to compare different degrader principles with each other. Therefore, we used a previously characterized Designed Ankyrin Repeat Protein (DARPin) that binds to GFP with high affinity, and was part of the extensive set studied earlier.[18] The DARPin can be fused or chemically cross-linked to all different degraders of this study. Third, to compare the potency of the different degraders, we have to overcome potentially large differences in cellular uptake between the different substance classes, even though the fusion to the DARPins makes them already more similar to each other. For this reason, we used microinjection into single cells,[18,20] which measures target protein degradation rates independent of either biosynthesis rates and/or uptake rates. It is based on automated live-cell microscopy to continuously assess the degradation rate, subcellular localization and intracellular concentration of protein analytes at the single-

https://doi.org/10.1021/acschembio.5c00569
ACS Chem. Biol. XXXX, XXX, XXX−XXX

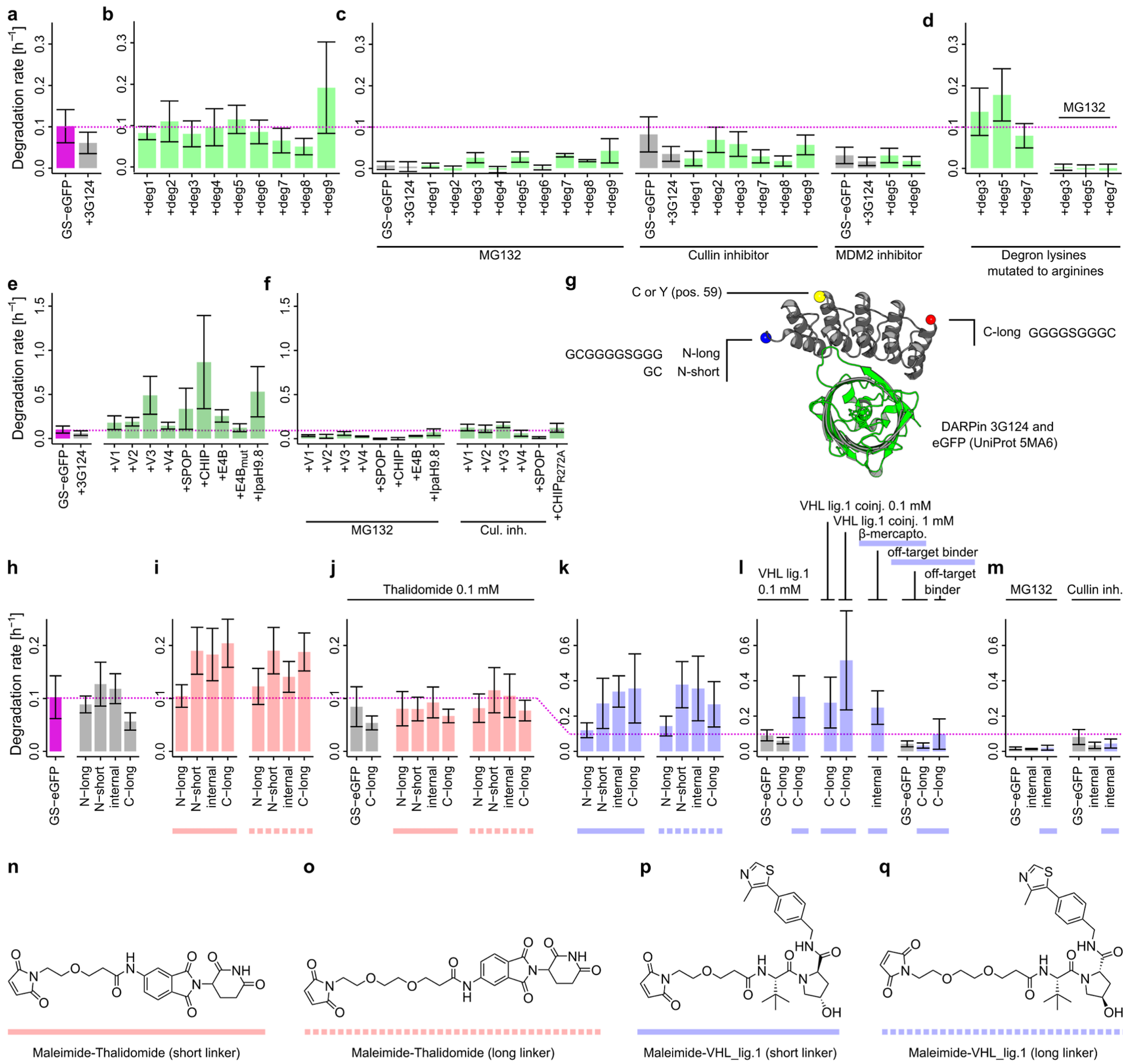

Figure 2. GS-eGFP degradation by DARPin-based bioPROTACs. (a−f) Average degradation rate constants of GS-eGFP alone or in a 1:1 complex with the indicated molecule, determined by microinjection into HEK293 cells. Error bars represent standard deviations. Numbers of analyzed cells per analyte are shown in Supporting Information Data 1. Since the *y*-axes of the different panels are different, a magenta dashed line indicates the degradation rate of GS-eGFP. Statistical significance between analyte degradation rates are shown in Figure S3. (a) GS-eGFP rate alone and in complex with DARPin 3G124 without fusion. (b,c) bioPROTACs containing unstructured peptides (degrons) fused to the C-terminus of DARPin 3G124 (sequences see Table 1), with or without the presence of the indicated inhibitors. (d) Peptide-based bioPROTACs where lysines were mutated to arginines, with and without proteasome inhibitor MG132. (e) bioPROTACs based on folded domains (see Table 1) fused C-terminally to DARPin 3G124. (f) The same constructs in the presence of inhibitors. (g) Structure of DARPin 3G124 in complex with eGFP. Shown are the variants containing different linkers and cysteines in different positions for the coupling of small molecules. (h−m) Median degradation rate constants of GS-eGFP alone, or in complex with eGFP-binding DARPin 3G124 variants containing different N- and C-terminal linkers before coupling, as well as coupled to thalidomide or VHL ligand 1. The coupling to Cys 59 is denoted as ″internal″. The structures of the coupled ligands are shown in (n−q) (see below). Rates were determined by microinjection into HEK293 cells. Error bars represent standard deviations. (h) 3G124 variant as shown in (g). (i,j) Thalidomide-based bioPROTACs with and without competitor thalidomide added to the cell medium before injection. (k−m) VHL ligand 1-based bioPROTACs with and without different indicated competitors (l) and inhibitors (m), for details on the compounds, see main text. (n−q) Maleimide-containing variants of pVHL- and CRBN-binding molecules for site-specific coupling to cys derivatives of DARPin 3G124. Shown are the CRBN (n,o) and pVHL-engaging (p,q) molecules. Two variations of each are shown, differing only in the length of the poly ethylene glycol (PEG) linker length. The lines under the structures (color and solid or dashed) are also used in the bar graphs (i−m). Statistical significance between degradation rates of different analytes are shown in Figure S3.

cell level. Cells are unperturbed and grown in unaltered environmental conditions and show high viability. The injection of analytes at defined ratios and concentrations allows for a clearly defined starting point of degradation,

Table 1. Overview of Peptide- and Protein-Based E3 Domains or Interaction Domains for Creation of bioPROTACs, Created as C-terminal Fusions to eGFP-Binding 3G124 with the Listed Linker

short name	source protein	engaged E3/complex	type	sequence/region	linker	MW [kDa]	PDB ID	used in PROTAC	lit	deg rate (h^{-1})
deg1	IκBα	CRL1$^{\beta\text{-TRCP}}$	degron	DRHDSGLDSM	G4S	1.1	-	yes	25,26	0.08
deg2	EID1	CRL1$^{\text{FBXO21}}$	degron	AFIEELFSLMVVN	G4S	1.5	-	no	27	0.11
deg3	RRM2	CRL1$^{\text{CyclinF}}$	degron	RGRRRRQR-G_4S-TRVLASKTARRIFQEPTEPKT	G4S	3.7	-	no	28	0.08
deg4	HIF-1α	CRL2$^{\text{VHL}}$	degron	MLAPYIMP	G4S	1.0	-	yes	29,30	0.10
deg5	P53	MDM2	degron	PLSSSVPSQKTYQGSYGFRKLG	G4S	2.4	-	no	31,32	0.12
deg6	P53 min seq	MDM2	degron	GSYG	G4S	0.4	-	no	33	0.09
deg7	iNOS	CRL5$^{\text{SPSB2}}$	degron	NGEKDINNNVE	G4S	1.2	-	no	34,35	0.07
deg8	synthetic	unknown	degron	TRGVEEVAEGVVLLRRRGN	G4S	2.1	-	no	32,36	0.05
deg9	synthetic min seq	CRL2	degron	RRRG	G4S	0.5	-	no	32,36,37	0.19
V1	OV128 (Orf virus)	CRL1	folded domain	473−500	G4S	3.1	-	no	38,39	0.18
V2	MYXV005 (myxoma virus)	CRL1	folded domain	454−483	G4S	3.6	-	no	38,40	0.19
V3	MVA186R (vaccinia virus)	CRL1	folded domain	544−574	G4S	3.6	-	no	38,41	0.49
V4	OV129 (Orf virus)	CRL1	folded domain	490−520	G4S	3.4	-	no	38,39	0.15
SPOP	SPOP	CRL3	folded domain	167−374 (UniProt ID O43791)	G4SG4S	23.1	8DWU	yes	16,21,42	0.34
CHIP	CHIP	CHIP homodimer	folded domain	128−303 (UniProt ID Q9UNE7)	GSGS	20.8	2C2L	yes	16,42−51	0.87
E4B	E4B	E4B monomer	folded domain	1227−1300 (UniProt ID O95155)	GSGS	8.6	3L1X	no	52	0.26
IpaH9.8	S. flexneri IpaH9.8	S. flexneri IpaH9.8	folded domain	254−545 (UniProt ID Q31SH3)	GSGS	33.4	6LOL	yes	53	0.53

without the entanglement of biosynthesis/uptake, often encountered in existing methods. We have also established the use of chemically coupled dyes as robust reporters for protein degradation,[18,20] and elucidated the significance of their membrane-permeability, thereby extending the applicability of our method to any protein of interest.

While one might argue that this direct measurement of the actual degradation rate is less relevant than an overall degradation that includes uptake as a variable, we believe it is essential to untangle the different components that determine the observed rates. Moreover, the direct injection gives a precise starting point of the degradation reaction.

While previous studies have compared different E3 domains qualitatively,[16,21] our focus here lies on measuring differences in specific degradation rates using our previously developed method based on microinjection and live-cell microscopy.[18,20] This strategy has permitted us to directly compare chemically coupled PROTACs with proteins and peptides for the same specificity. Our findings may serve as a foundation for understanding degradation processes and hold potential therapeutic implications in the future.

RESULTS

Comparison of bioPROTAC Design Strategies to Induce E3 Interaction

We aimed at comparing different UPS interaction domains for the construction of bioPROTACs and the subsequent degradation of the proof-of-principle target eGFP. In all cases, the interaction partner with GFP was a DARPin[22] whose structure in the complex was known. Since wt GFP is hardly degraded over 24 h, we added an N-terminal extension of two amino acids, Gly−Ser, required for efficient proteasomal unfolding. This N-terminal GS tag brings the natural degradation rate of GS-eGFP to 7 h in the absence of added PROTACs or bioPROTACs (Figure 2a,h), as described previously.[20] Therefore, both the acceleration and the inhibition of degradation can be monitored. While other longer tags can be added that accelerate the degradation of GFP,[20,23,24] here we were interested in only relative comparisons of degradation rates and wanted to minimize the possibility that a sequence intended to be an unfolding initiation site can also act as a degron, thereby obscuring the investigations of the degrons of interest.

To assess induced degradation rates of GS-eGFP upon interaction with by DARPin-based bioPROTACs, we have used our recently developed approach combining microinjection with live-cell fluorescence microscopy.[20] Videos of the microinjection and cell viability can be found in the Supplement of ref 20 and examples of individual degradation rates and their conversion to the bar graphs used throughout these studies is shown in Figure 1d−f of ref 18. The use of this approach reduces the effects of external variables such as differences in membrane permeability, which often leads to unknown cytosolic bioPROTAC concentrations as well as additional slow steps, complicating the measurements of true degradation rates. To reduce the influence of other confounding factors such as variable target engagement and/or premature degradation of the bioPROTACs themselves, we formed bioPROTAC/GS-eGFP complexes in a 1:1 ratio through mixing and subsequent purification of the complexes using size-exclusion chromatography (see Methods). These preparations ensured the detection of differences based solely

https://doi.org/10.1021/acschembio.5c00569
ACS Chem. Biol. XXXX, XXX, XXX−XXX

from UPS-engagement and subsequent proteasomal degradation. Tag-free purified proteins were obtained using a protease-cleavage and multicolumn chromatography strategy (see Methods). Quality control was conducted via mass spectrometry, as shown in Figures S1 and S2.

We compared three classes of UPS recruitment domains for bioPROTAC design: Unstructured peptides (degrons) that get recognized by an E3 or E3 complex, folded protein domains that are part of, or can recruit an E3 complex and two small-molecule ligands for E3 ligases. The peptide or protein-based constructs can generally be grouped according to their size, structural type, biological origin, or prior usage for PROTAC design, as shown in Table 1. Sequences of all constructs are shown in Supporting Information Data 1. Degron and E3 domains were genetically fused to the C-terminus of the eGFP-binding DARPin 3G124.[22] For the small-molecule-based bioPROTACs, the ligands were synthesized to contain a maleimide group and could be coupled to different unique cysteines introduced to DARPin 3G124, as shown in Figure 2g, to assess the impact of positioning and different linker length on degradation. The results of the three strategies will be discussed in detail in the following sections. Analyzed cell numbers, mean rates, standard deviation and single cell rates of all injected analytes are shown in Supporting Information Data 2. Statistical significance values between degradation rates of different analytes are shown in Figure S3.

Degron-Based UPS-Targeting Domains

To evaluate the efficacy of degron-based bioPROTACs, we employed nine published degron sequences (deg1 to deg9 (Table 1)), several of which have been successfully utilized in PROTACs in prior studies. These degrons were tested to compare their degradation-inducing propensity against each other and with strategies employing E3 ligase domains or small-molecule warheads. Overall, degron-based bioPROTACs yielded lower target degradation rates compared to the other two strategies (Figure 2). However, for most of the nine tested degron constructs, target degradation was enhanced relative to the DARPin 3G124/GS-eGFP complex lacking a fused degron domain, which decreases the degradation rate of GS-eGFP. Importantly, most of the degron constructs did not achieve degradation levels exceeding those observed for the target protein GS-eGFP in isolation. Among the constructs, the highest enhancement in degradation was observed with construct deg9, which notably reduced the target protein's half-life from 7 to 3.6 h (degradation rate 0.10 to 0.19 h^{-1}). Deg9 is a synthetic peptide featuring a sequence motif previously associated with C-terminal degrons, thus suggesting potential interaction with Cullin 2 RING E3 ligase (CRL2) complex.[37] We found that degradation of GS-eGFP by deg9 could indeed be inhibited by the Cullin inhibitor MLN4924,[54] indicating a Cullin-based mechanism. All degron-constructs could also be inhibited by proteasome inhibitor MG132, thus demonstrating a proteasome-dependent degradation mechanism (Figure 2c).

It has been proposed that an unstructured tail is needed for successful proteasomal unfolding.[55] The increased degradation rate facilitated by degron peptides may therefore also stem from their ability to provide initiation sites for proteasomal unfolding, rather than solely functioning as binding sites for E3 ligases. However, degradation kinetics were found to be decreased by pathway-specific inhibitor treatment, suggesting indeed the recruitment of the proposed E3-ligase for degradation (Figure 2c). It is of note, however, that 3G124/GS-eGFP complexes were inhibited by both a Cullin inhibitor and the MDM2 inhibitor MEL23,[56] independent of the C-terminal degron fusion (Figure 2c). DARPin 3G124 itself could thus also provide potential E3 binding sites.

We next tested whether lysines in the degrons promote degradation by providing an additional potential ubiquitination site, independent of the proposed degron/E3 mechanism. For this purpose, the lysines within the degrons were mutated to arginines. Surprisingly, the substitution of lysines to arginines *increased* degradation rates of all three degrader/GS-eGFP complexes which contained them, suggesting that these lysines are not relevant ubiquitination sites (Figure 2d). Possibly, the affinity between E3 or the proteasome and degron was increased or the respective E3 mechanism changes upon lysine mutation.

Several factors could contribute to the limited efficacy of most degron peptides. One consideration is their typically low stability, rendering them prone to proteolytic degradation. Consequently, this vulnerability may compromise the effectiveness of bioPROTACs employing these peptides as a strategy. Additionally, the fusion of degron peptides to the C-terminal end of DARPin could hinder the binding of a E3 ligase due to the specific steric requirements of the respective ligase. Moreover, the precise positioning of the E3 binding site may constrain the accessibility of specific lysines on GS-eGFP necessary for its degradation. In a study conducted by Melvin et al.,[33] it was observed that the efficacy of degrons deg5 and deg6 (Table 1 and Figure 2c) was contingent upon the position of a lysine residue N-terminal to the degron sequence. Optimal degradation was achieved when the lysine was located proximal to the N-terminus of the degron sequence. This spatial requirement may not be compatible with the specific bioPROTAC/GS-eGFP complexes tested in our investigation, potentially partially explaining the diminished degradation of GS-eGFP observed with these degrons.

An additional factor contributing to the efficacy of degron peptides is the potential requirement for post-translational modifications to facilitate interaction with E3 ligases. In the original study introducing the first ever PROTAC, Protac-1, incorporating the deg1 degron, phosphorylation of serine residues was performed in vitro and ubiquitination tested in HEK293T lysate and *Xenopus* extracts.[25] However, it remains uncertain whether phosphorylation can occur intracellularly after microinjection. Deg3 has also been proposed to necessitate phosphorylation of a specific threonine residue for effective E3 interaction, which is not included in the used sequence.[28] However, interaction with RRM2 was also shown to occur without this phosphorylated site but might be less affine. Furthermore, post-translational modification may be essential for the functionality of deg4, a peptide derived from HIF-1α.[29] Under normoxic conditions, HIF-1α degradation is initiated by the hydroxylation of Pro564, a conserved proline residue, facilitating recognition by the CRL2 E3 ligase.[57] Successful degradation was observed by Montrose and Krissansen[30] using the deg4 peptide without prior hydroxylation in a cell-permeable PROTAC on HepG2 cells, but it remains unclear whether hydroxylation can occur subsequent to introduction to the cellular environments. In light of the observed low degradation rates within our experimental framework, the occurrence of hydroxylation remains uncertain.

https://doi.org/10.1021/acschembio.5c00569
ACS Chem. Biol. XXXX, XXX, XXX−XXX

Protein-Based UPS-Targeting Domains

For protein-based UPS-targeting strategies, we employed a range of E3 ligase domains, including several previously characterized domains as well as novel domains not yet explored in the context of targeted protein degradation (Table 1 V1 to IpaH9.8). Among the established E3 ligase domains, we examined the Speckle-type BTB−POZ protein (SPOP) domain interacting with CRL3,[16,21,42] C-terminus of Hsc70-interacting protein (CHIP), a Ubox-type E3 ligase[16,42−51] and the bacterial E3 ligase IpaH9.8 from *Shigella flexneri*.[53] For our exploration of novel E3 ligase domains, we investigated a monomeric E3 member of the Ubox family, E4B,[52] because its smaller size could be attractive for intracellular delivery methods relying on refolding of proteins.[58] Furthermore, we examined four F-box-like protein domains (V1 to V4, Table 1), derived from viral proteins[38] that were shown to interact with the Skp, Cullin, F-box containing complex (SCF complex, also called CRL1) E3 ligase.[39−41,59] The viral proteins were chosen since their hijacking of host E3 mechanisms might have evolved to an increased efficiency and stability, through evolutionary selection of the viruses.

All protein-based bioPROTACs were found to be effective in increasing GS-eGFP degradation but to starkly different degrees (Figure 2e). The best-performing E3 domains were V3, an F-box domain from vaccinia virus, SPOP, IpaH9.8 and CHIP. Measurements with proteasomal inhibition by MG132 further showed that the observed degradation was indeed produced by a proteasomal degradation mechanism (Figure 2f).

The protein domain CHIP produced the highest degradation rate out of all tested bioPROTACs and modulated the half-life from 7 h to approximately 48 min (deg. rate from 0.10 to 0.87 h^{-1}). It has been proposed that the high flexibility of CHIP allows for efficient ubiquitination of residues at varying distance, which could explain the high degradation rate.[60] We could further confirm that the observed degradation is indeed caused by CHIP activity, since injection of an analogous bioPROTAC with CHIP containing the mutation R272A, which abolishes E2 interaction and degradation (Figure 2f), did not increase GS-eGFP degradation.

The Cul3 adapter protein SPOP was the fourth most efficient in inducing the degradation of GS-eGFP, reducing its half-life from 7 to approximately 2 h (deg. rate from 0.10 to 0.34 h^{-1}). These results support previous studies by Shin et al.[21] and Lim et al.,[16] wherein SPOP was identified as either the most efficient or one of the most potent strategies among the tested domains. Notably, by quantifying degradation rates rather than simply monitoring target levels over time, we demonstrate here that CHIP actually surpasses SPOP in effectiveness. Importantly, degradation by the SPOP-based bioPROTAC could be greatly reduced by a Cullin inhibitor, thus confirming the proposed Cullin3-Ring E3 ligase-based mechanism.[61]

The protein domain inducing the second highest degradation rate of GS-eGFP was IpaH9.8, modulating GS-eGFP half-life from 7 to approximately 1.3 h (deg. rate from 0.10 to 0.53 h^{-1}). This very efficient degradation induction is in line with findings by Ludwicki et al.,[53] who tested a panel of different bacterial E3 ligase mimics for bioPROTAC generation and found that IpaH9.8 was the most potent degradation-inducing domain.

Among the four protein domains (V1 to V4, Table 1) derived from viral proteins with F-box-like domain,[38] the one from vaccinia virus (V3) stands out, as it resulted in a significant reduction of the GS-eGFP half-life from 7 to 1.4 h (deg. rate from 0.10 to 0.49 h^{-1}). Consequently, this strategy ranks as the third most effective bioPROTAC among all tested approaches. Conversely, other viral F-box-like proteins (V1, V2, V4, Table 1) showed only slight increase in GS-eGFP degradation. The viral proteins selected for investigation here, owing to them possessing F-box-like domains, were hypothesized to engage with SCF ubiquitin ligase (CRL1) complexes[38], and indeed it was later shown that all four viral proteins, from which the F-box-like domains V1−4 were derived, likely interact with SCF component Skp1.[39−41] Our findings support this hypothesis, as degradation was decreased upon the addition of a Cullin inhibitor. The underlying mechanisms driving the variable efficacy of these constructs in modulating degradation rates still remain to be fully elucidated, but may depend upon their distinct interactions with the SCF complex.

In contrast to the highly effective Ubox-type CHIP E3 ligase strategy, the smaller monomeric Ubox-type E4B produced a much lower increase in GS-eGFP degradation. This difference in efficacy may stem from limitations of flexibility in combination with the spatial arrangement of residues available for ubiquitination on GS-eGFP. A mutant version of E4B reported by Park et al.,[62] denoted "E4BU(#8)" (here termed $E4B_{mut}$), showed an increased ubiquitination rate in vitro and has been proposed as a promising candidate for bioPROTAC generation. We tested if this variant would also be more efficient at GS-eGFP degradation in vivo. Microinjection revealed, however, that the GS-eGFP degradation rate with this variant ($E4B_{mut}$) was even lower than that of E4B wild type (Figure 2e). The mutations might cause instability or binding of other cellular proteins which possibly reduces ubiquitination efficiency.

Small-Molecule-Based UPS-Targeting Domains

We chose two small molecules to engage with E3-pathways: (1) VHL-ligand-1, which interacts with the substrate recognition component of the Cullin-2 E3 complex (pVHL)[63] and (2) thalidomide/pomalidomide which interacts with cereblon (CRBN) that is part of the Cullin-4A E3 complex.[64,65] Both compounds were synthesized with two PEG linkers of different length (Figure 2n−q) and maleimide, and attached to a unique cysteine, introduced either directly at the N- or C-terminus of DARPin 3G124 or separated by a Gly−Ser linker (Figure 2g). Additionally, we introduced a coupling site at the "backside" of the DARPin, away from the binding site to GFP, by introducing the mutation Y59C denoting the coupling as "internal" (Figure 2h−l). Given that successful ubiquitination is dependent on both spatial proximity and orientation of the E2 catalytic center and ubiquitination sites,[66] we thus changed the linker length both within the small molecule and in the protein (Figure 2g,n−q). Successful production of PROTACs was assessed using ESI-MS, and it confirmed complete coupling for most samples, as shown in Figure S1.

In the absence of a coupled small-molecule, the introduction of single-cysteines by the addition of either of the two N-terminal linkers or internal mutation Y59C in DARPin 3G124 did not alter GS-eGFP degradation rates (Figure 2h). However, the introduction of a C-terminal 9-amino acid long linker increased the half-life of GS-eGFP from 6 to 11.6 h (deg. rate from 0.10 to 0.06 h^{-1}). When coupling the two small

https://doi.org/10.1021/acschembio.5c00569
ACS Chem. Biol. XXXX, XXX, XXX−XXX

molecules, none of the PROTACs based on the conjugation to an N-terminally located 10-amino acid long linker were able to induce GS-eGFP degradation, independent of using thalidomide or VHL ligand 1, and thus testing the two involved pathways, and independent of PEG linker length. This could be caused by an unfavorable geometry of the recruited complex to ubiquitination sites on GS-eGFP. Conjugation to all other cysteine locations resulted in PROTACs inducing GS-eGFP degradation, although with different efficiencies.

All active thalidomide-based bioPROTACs showed similar effectiveness and reduced the GS-eGFP half-life to 3.6 h (deg. rate from 0.10 to 0.19 h^{-1}), with the exception of a construct containing thalidomide with a longer PEG linker positioned internally, which induced a slightly slower half-life reduction to 5.0 h (deg. rate 0.14 h^{-1}). The addition of free thalidomide to the surrounding medium brought degradation down to background levels of GS-GFP alone, which is consistent with the expected competition to the CRBN binding site. The VHL-ligand-1-based bioPROTACs generally showed higher activity than the thalidomide ones, with the strongest effect resulting in a 2.0 h half-life (deg. rate around 0.35 h^{-1}), and only minor differences between constructs. Since both warheads bind their target E3 components with similar affinities in the high nanomolar range,[63,64] differences may arise due to varying complex recruitment or ubiquitination efficiency.

Unfortunately, our attempts to verify the distinct recruitment mechanism of the VHL-ligand-1 constructs were inconclusive when employing direct competition assays with either VHL-ligand-1 (termed ″VHL lig.1″) or the maleimide-VHL-ligand-1 construct quenched with β-mercaptoethanol to simulate a product closer to the protein conjugate (Figure 2l, termed ″β-mercapto″), since no clear inhibition was observed. Furthermore, competition experiments involving a non-GFP-binding DARPin, bearing a C-terminal long linker coupled to the VHL-ligand-1 construct (Figure 2l, termed ″off-target binder″), did not produce conclusive results, as the coinjection of even 25 μM of this nonbinding DARPin, with and without any attached small molecule, still resulted in a decrease in GS-eGFP degradation for one 3G124-VHL-ligand-1/GS-eGFP complex, potentially due to overloading of the cellular proteasomal system. We can therefore show that the DARPin-VHL-ligand-1 conjugates lead to enhanced degradation (Figure 2k), but not that they work exclusively by engaging VHL. Nonetheless, our findings unequivocally demonstrate the proteasome-dependence of degradation mediated by the VHL-ligand-1 strategy, as evidenced by the substantial reduction in degradation upon addition of the proteasome inhibitor MG132 (Figure 2m). Additionally, the decrease in degradation observed upon the addition of a Cullin inhibitor strongly suggests degradation by a Cullin-based degradation mechanism, consistent with the proposed recruitment of Cullin-2 by the targeted pVHL (Figure 2m).

■ DISCUSSION

With the increasing interest in PROTAC and bioPROTAC development, various E3-hijacking strategies have been identified,[8−17,19,67] but a comparison based solely on accelerating degradation is lacking in most cases. To evaluate such experiments, it would be necessary to take into account the influence of binding affinity to the target, degradation rate before target engagement by other cellular degradation mechanisms, and the functional steady-state level of the PROTAC, given by the rate of bioPROTAC biosynthesis and folding efficiency, or the rate and success of intracellular delivery if it is added from the extracellular milieu. By measuring degradation rates of preformed bioPROTAC/GS-eGFP complexes in HEK293 cells under the same conditions, we were able to obtain a fair comparison between different E3 recruitment strategies and the same eGFP-binding DARPin. Importantly, the direct measurement of degradation rates with a defined starting point—independent of confounding parameters—permits this comparison, even across small molecules, peptides and protein domains.

Most of the investigated degron peptides showed lower degradation rates compared to protein-domain and small-molecule strategies. This discrepancy may stem from the requirement for additional modifications necessary for efficient binding of these peptides to their respective E3 ligases, which were not included in our investigation. However, one synthetic peptide bearing the sequence RRRG induced rapid degradation of GS-GFP, likely by being targeted by CRL2,[37] as we detected a lower degradation when adding a Cullin inhibitor. The CHIP E3 ligase domain yielded the highest degradation rate among the tested constructs, while the IpaH9.8 an E3 ligase mimic from *S. flexneri* which is a V3 protein domain, and the F-box-like protein from vaccinia virus, ranked second and third. In contrast, other F-box-like proteins from various viruses had negligible effects on degradation. SPOP also exhibited relatively high degradation rates, consistent with previous reports of its effectiveness.[16,21] Contrary to expectations, reported mutations aimed at enhancing the in vitro ubiquitination ability of the small Ubox-type E3 ligase E4B[62] resulted instead in decreased degradation rates in HEK293 cells.

A comparison of the two small-molecule-based degradation strategies revealed that VHL-ligand-1 generally induced higher degradation rates than thalidomide. Furthermore, both the placement on the protein and length of the linker were important, as N-terminal coupling to the DARPin with a long linker abolished degradation of GS-GFP, while variations in degradation were minor for other linker lengths and positions. We successfully demonstrated pathway-specific inhibition for all tested strategies except for pVHL targeting by VHL-ligand-1. While we confirmed proteasome and Cullin-dependent degradation by the pronounced effect of the corresponding inhibitors, further experiments are needed to elucidate the specific pathways involved.

Differences in the expression of E3 complex components may elucidate the variability in degradation rates observed among the tested strategies. To investigate this, RNA expression levels of E3 complex components necessary for bioPROTAC functionality were obtained from the Human Protein Atlas (Table ST1). Our analysis revealed that all components are expressed in HEK293 cells at levels that are either higher than or close to the median RNA expression levels, thereby excluding the possibility that the failure of certain strategies is due to the lack of expression of essential components. Nonetheless, it is important to consider that RNA expression levels may not reflect translation rates or actual protein levels. Additionally, even low expression levels of certain components may be sufficient due to the enzymatic activity of the E3 complex.

The high degradation rates achieved by degron deg9 (the short sequence RRRG) and the small-molecule strategies suggest their potential as promising candidates for intracellular

https://doi.org/10.1021/acschembio.5c00569
ACS Chem. Biol. XXXX, XXX, XXX−XXX

delivery, e.g. via a bacterial toxin-based mechanism, as this approach avoids the need for peptide refolding, and the DARPins have been shown before to refold successfully in such an approach.[68] Similarly, the compact sizes of protein domains V3 and E4B make them intriguing candidates, as their smaller dimensions may facilitate refolding processes. An example of the cytosolic delivery of a bioPROTAC, consisting of a monobody conjugated with a VHL-binding small molecule, recently was achieved through a mechanism dependent on ETA bacterial toxin.[69] In addition to bacterial toxin-based mechanisms, gene delivery strategies, which have gained traction in recent years,[70] offer a versatile approach for delivering bioPROTACs independent of their size, however, this is not compatible with chemical conjugates. Taken together, these delivery approaches expand the potential therapeutic applications of bioPROTACs. Our results can therefore contribute to the selection of the most effective E3 domains for bioPROTAC design, thereby facilitating their development for investigational and eventual therapeutic use.

The present study has potential limitations. We only investigated one cell line, HEK293, and the protein expression levels of the components of the UPS may be limiting certain degradation pathways, even though the RNA levels appear to be sufficient (see above and Table S1). Also, the uptake was achieved by microinjection to obtain degradation rates unencumbered by different uptake rates. Therefore, the actual uptake will have to be studied for the most promising constructs and in a separate set of experiments. While in the present manuscript the focus was on the comparison of different types of degradation domains, we have shown in our previous work that ubiquitination is directly involved in degradation and the rates are consistent with more traditional (and less accurate) quantification with Western blots.[18,20]

In conclusion, these results can inform the design of next-generation bioPROTACS. For example, none of the peptide degrons showed impressive degradation rates, and while there are many more peptide degrons which have not been tested, it may seem less attractive to work on such constructs. The small-molecule conjugates of thalidomide and VHL-ligand-1 reach similar degradation rates as the E3 fusions, and thus their preferred use may also depend on the ease of administration.

■ METHODS

Design and Cloning of Expression Constructs

Proteins were expressed from the pQIq vector (a lacI^q-encoding derivative of pQE30; Qiagen, Hilden, Germany)[71] that encodes an N-terminal MRGS-His tag, followed by an Avi-tag and TEV cleavage site in front of the DARPin. When additional N-terminal fragments (single cysteines with and without Gly−Ser linker) were used, they were inserted by *Eco*RI/*Bam*HI sites. The fragment coding for the DARPin 3G124 was inserted via *Bam*HI/*Pst*I sites. C-terminal fragments (Gly−Ser linkers with single cysteines, linkers followed by the peptides or domains in Table 1) were inserted by *Pst*I/*Hin*dIII sites. Fragments were synthesized by Integrated DNA Technologies (IDT) and Twist Bioscience.

Protein Expression and Purification

The *E. coli* strain BL21 was used for expression. Constructs containing a single-cysteine for small-molecule coupling and bioPROTAC constructs with a viral F-box like protein E3 domain were expressed by induction with 400 μM IPTG in 1 L TB-medium. Cells were grown at 37 °C until an OD600 of approximately 1.5 was reached. For single cysteine constructs, the temperature was then reduced to 25 °C and expression was performed for 16 h. The DARPin with an introduced internal cysteine at position 59 and all other bioPROTACs were expressed by autoinduction in 1 L autoinduction medium[72] at 25 °C for 24 h. Cells were harvested by centrifugation at 4 °C. Lysis buffer (50 mM Tris, 500 mM NaCl, 10% w/v glycerol, 0.5 mM EDTA, 0.2 mM AEBSF, 1.4 μM Pepstatin-A, 1 μM Leupeptin and 1 mg mL^{-1} lysozyme, pH 8 at 4 °C) was added and cells were lysed with a French press. The supernatant was cleared by ultra-centrifugation at 20,000 *g* at 4 °C. Bench-top IMAC was performed with 5 mL Ni-NTA bed volume in running buffer (50 mM Tris, 500 mM NaCl, pH 8 at 4 °C). Bound protein was washed with running buffer and wash buffer (50 mM Tris, 500 mM NaCl, 10 mM imidazole, pH 8 at 4 °C) before elution with elution buffer (50 mM Tris, 500 mM NaCl, 250 mM imidazole, pH 8 at 4 °C). Proteins were buffer-exchanged by overnight dialysis at 4 °C against dialysis buffer (20 mM Tris, 100 mM NaCl, 1 mM DTT, pH 8 at 4 °C) with simultaneous TEV cleavage at a molar ratio of 1:10. Samples were reduced before dialysis with 10 mM DTT for 30 min. Uncleaved protein and His-tagged TEV was removed by benchtop reverse IMAC with dialysis buffer. Protein samples were diluted 1:1 with MQ water for subsequent anion exchange chromatography using a MonoQ 5/50 GL column on an ÄKTA pure™ system. Protein was loaded using AEX running buffer (10 mM Tris, 50 mM NaCl, pH 8 at 4 °C) and eluted by gradient elution from 0 to 100% elution buffer (10 mM Tris, 500 mM NaCl, pH 8 at 4 °C) in 40 CV. Samples were pooled and flash-frozen in liquid nitrogen for storage at −80 °C.

Synthesis of Compounds

The synthetic methods are described in the Supplementary Methods.

Coupling of Compounds

200 μL protein was incubated with 10 mM DTT for 30 min at RT. The buffer was exchanged to degassed PBS pH 6.8 with added 1 mM EDTA using a PD MiniTrap G-25 column (Cytiva) in an N_2 atmosphere. Compounds (synthesized at and received from the Crews lab) at 25 mM in DMSO were added in a 3.5 molar excess and incubated for 3 h at RT with shaking at 550 rpm. The reaction was quenched with 100 mM DTT for 10 min and flash-frozen in liquid nitrogen for storage at −80 °C until further use.

eGFP Complexation

eGFP complexes were formed by mixing coupled binders with eGFP in a molar ratio of 1.5:1 of the smaller to higher molecular weight species. Equimolar (1:1) complexes were purified by size-exclusion chromatography (SEC) in PBS (pH 7.5) using either a Superdex 75 10/300 GL or Superdex 200 10/300 GL column on an ÄKTA pure™ system. Eluted fractions were pooled and flash-frozen in liquid nitrogen for storage at −80 °C.

ESI-MS

Mass spectrometry analyses were carried out at the Functional Genomics Center Zurich. For ESI-MS analysis, samples were diluted 3-fold with 1% TFA and transferred to an autosampler vial for LC/MS. Seven μL of sample were injected into an Acquity UPLC with a BioResolve-RP-mAb 2.7 μm, 2.1 × 150 mm, 450 Å column (Waters, USA). For separation and elution on an Acquity UPLC station, a gradient of buffer A (0.1% DFA in water)/buffer B (0.1% DFA in AN/75% 2-PrOH) at a flow rate 200 μL/min at 60 °C was applied for 10 min. The analysis was performed on a Synapt G2 mass spectrometer directly coupled to the UPLC station. Mass spectra were acquired in the positive-ion mode by scanning the m/z range from 400 to 5000 Da with a scan duration of 1 s and an interscan delay of 0.1 s. The spray voltage was set to 3 kV, the cone voltage to 35 V, and the source temperature to 100 °C. The data were recorded with the MassLynx 4.2 Software (Waters, UK). Where possible, the recorded m/z data of single peaks were deconvoluted into mass spectra by applying the maximum entropy algorithm MaxEnt1 (MaxLynx) with a resolution of the output mass 0.5 Da/channel and Uniform Gaussian Damage Model at the half height of 0.5 Da.

Cell Culture

HEK293 cells (ATCC CRL-1573) were maintained in DMEM supplemented with 10% heat-inactivated fetal calf serum (FCS) and 1% (v/v) penicillin/streptomycin. Cultures were incubated at 37 °C

https://doi.org/10.1021/acschembio.5c00569
ACS Chem. Biol. XXXX, XXX, XXX−XXX

in a humidified atmosphere with 5% CO_2 using 75 cm^2 plates. Cells were passaged every 4−5 days by trypsinization and reseeded at a 1:20 dilution.

Microinjection and Live-Cell Imaging

Microinjection experiments were conducted as previously described.[20] Briefly, HEK293 cells were seeded into microscopy dishes 2 days prior to injection to achieve 80−90% confluency on the day of the experiment. Four hours before microinjection, the culture medium was replaced with Live Cell Imaging Solution (Invitrogen) supplemented with 10% fetal calf serum (FCS).

Analyte solutions were prepared at a final concentration of 25 μM and included 0.1 mM Alexa Fluor 647-labeled dextran (10 kDa; #D22914, Invitrogen) as an injection marker.[20] Microinjections were performed using an InjectMan4 and FemtoJet4i system (Eppendorf) equipped with Femtotip II glass capillaries (Eppendorf). Manual injections were carried out for approximately 30−100 cells per analyte, with flow controlled by manually inserting and withdrawing the capillary from individual cells. This approach led to variability in both injected volume and intracellular concentration. Importantly, degradation rates were previously determined to be independent of the initial injected concentration and injection volume.[20] Briefly, the injection volume is recorded by using the integrated fluorescence of the injection marker, and it is described by a Weibull distribution, with the most frequently injected volume of 25 μm^3, corresponding to 1.7% of the volume of a HEK293 cell, and thus a 56-fold dilution.[20] The cells show high viability, with 75% of the successfully microinjected cells, 75% being available for single-cell analysis after 12 h observation, as evaluated by comparing data from over 30 independent experiments.[20]

For competition and inhibition experiments, molecules were added to the injection medium 1 h prior to injection. Competitors were either 100 μM Thalidomide (T150, Sigma) or varying amounts of VHL-ligand-1 (21591, Cayman). Inhibitors were 10 μM MG132 (M8699, Sigma), 2 μM Cullin inhibitor MLN4924[73] (5.05477, Sigma) or 28 μM MDM2 Inhibitor VII, MEL23 (373227, Sigma).

Live-cell imaging was performed at RT during microinjection and subsequently at 37 °C using a Visitron CSU-W1 spinning disk confocal microscope equipped with up to four epifluorescence excitation channels (405, 488, 561, and 640 nm). Images were acquired every 20 min over a 12 h period.

Approximately 75% of the injected cells (typically 20−40 cells, most often ∼30) were suitable for analysis. Cells undergoing mitosis, exhibiting abnormal motility or morphology, or detaching from the substrate were excluded. Image preprocessing included flat-field and dark-field correction. Cell boundaries were automatically segmented using the injection marker channel in CellProfiler, and total cellular fluorescence was quantified at each time point.

Single-cell degradation rates (k) were derived by fitting an exponential decay function (eq 1) to fluorescence intensity data using the nonlinear least-squares (NLS) method in RStudio

$$y = y(0)\cdot e^{-kt} \tag{1}$$

Outliers in the degradation rates for each fluorescence channel (405, 488, 561, and 640 nm) were identified and excluded using the interquartile range (IQR) method in RStudio, retaining only values within [Q1 − 1.5 × IQR, Q3 + 1.5 × IQR]. The total number of analyzed cells and the number of retained rates are reported in Supporting Information Data 2. Mean and standard deviation values for each analyte were calculated using RStudio.

ASSOCIATED CONTENT

Data Availability Statement

All protein sequences are included within this paper's Supporting Information files. Source data for the graphs shown in this paper and underlying single-cell degradation rates are included in the Supporting Information files. Code for single-cell degradation rate analysis was deposited on GitHub and can be accessed at https://github.com/theplueckthunlab/2024_paper_microinjection.

Supporting Information

The Supporting Information is available free of charge at https://pubs.acs.org/doi/10.1021/acschembio.5c00569.

Additional methods on compound synthesis, additional experimental details; mass spectra; statistical significance; data from Human Protein Atlas (PDF)

Supporting Information Data 1 (XLSX)

Supporting Information Data 2 (XLSX)

AUTHOR INFORMATION

Corresponding Author

Andreas Plückthun − *Department of Biochemistry, University of Zurich, Zurich 8057, Switzerland;* orcid.org/0000-0003-4191-5306; Phone: +41 44 635 5570; Email: plueckthun@bioc.uzh.ch

Authors

David Vukovic − *Department of Biochemistry, University of Zurich, Zurich 8057, Switzerland*

Dorothea Winkelvoß − *Department of Biochemistry, University of Zurich, Zurich 8057, Switzerland*

Anto Udovcic − *Department of Biochemistry, University of Zurich, Zurich 8057, Switzerland*

Luca Riermeier − *Department of Biochemistry, University of Zurich, Zurich 8057, Switzerland*

Saul Jaime-Figueroa − *Departments of Molecular, Cellular and Developmental Biology; Chemistry; Pharmacology, Yale University, New Haven, Connecticut 06520-8103, United States*

Craig M. Crews − *Departments of Molecular, Cellular and Developmental Biology; Chemistry; Pharmacology, Yale University, New Haven, Connecticut 06520-8103, United States;* orcid.org/0000-0002-8456-2005

Complete contact information is available at: https://pubs.acs.org/10.1021/acschembio.5c00569

Author Contributions

[§]D.V. and D.W. authors contributed equally. D.V. and D.W. jointly designed experiments. D.V. and D.W. performed microinjection experiments. D.V. performed analysis of microinjection and ESI-MS experiments. L.R., A.U, D.V., D.W. purified proteins. C.M.C. and S.J.-F. synthesized thalidomide and pVHL-derivatives for bioconjugation. A.U and D.W performed maleimide coupling. A.P., D.V., D.W. wrote the manuscript. D.V. and D.W. designed figures. A.P. provided input, critical feedback, and guidance.

Notes

The authors declare no competing financial interest.

ACKNOWLEDGMENTS

This project was funded by the Schweizerische Nationalfonds, grant 310030_192689 (to A.P.) and the NIH, grant R35CA197589 (to C.M.C.). We are grateful for our collaboration with the Center for Microscopy and Image Analysis (ZMB), and especially Dr. Jana Döhner and Dr. Urs Ziegler, who not only provided continuous nightly microscope access, but also valuable technical advice. We are grateful to the Functional Genomics Center Zurich for proteomics analyses, and in particular Dr. Serge Chesnov, for ESI-MS analysis of purified proteins.

REFERENCES

(1) Glickman, M. H.; Ciechanover, A. The ubiquitin-proteasome proteolytic pathway: destruction for the sake of construction. *Physiol. Rev.* **2002**, *82* (2), 373−428.

(2) Ciechanover, A. Intracellular protein degradation: from a vague idea, through the lysosome and the ubiquitin-proteasome system, and onto human diseases and drug targeting (Nobel lecture). *Angew. Chem., Int. Ed. Engl.* **2005**, *44* (37), 5944−5967.

(3) Yen, H. C.; Xu, Q.; Chou, D. M.; Zhao, Z.; Elledge, S. J. Global protein stability profiling in mammalian cells. *Science* **2008**, *322* (5903), 918−923.

(4) Luh, L. M.; Scheib, U.; Juenemann, K.; Wortmann, L.; Brands, M.; Cromm, P. M. Prey for the proteasome: targeted protein degradation—a medicinal chemist's perspective. *Angew. Chem., Int. Ed. Engl.* **2020**, *59* (36), 15448−15466.

(5) Li, K.; Crews, C. M. PROTACs: past, present and future. *Chem. Soc. Rev.* **2022**, *51* (12), 5214−5236.

(6) Schapira, M.; Calabrese, M. F.; Bullock, A. N.; Crews, C. M. Targeted protein degradation: expanding the toolbox. *Nat. Rev. Drug Discovery* **2019**, *18* (12), 949−963.

(7) Wang, Z.; Liu, J.; Qiu, X.; Zhang, D.; Inuzuka, H.; Chen, L.; Chen, H.; Xie, L.; Kaniskan, H. U.; Chen, X.; et al. Methylated nucleotide-based proteolysis-targeting chimera enables targeted degradation of Methyl-CpG-Binding Protein 2. *J. Am. Chem. Soc.* **2023**, *145* (40), 21871−21878.

(8) VanDyke, D.; Taylor, J. D.; Kaeo, K. J.; Hunt, J.; Spangler, J. B. Biologics-based degraders - an expanding toolkit for targeted-protein degradation. *Curr. Opin. Biotechnol.* **2022**, *78*, 102807.

(9) VanDyke, D.; Xu, L.; Sargunas, P. R.; Gilbreth, R. N.; Baca, M.; Gao, C.; Hunt, J.; Spangler, J. B. Redirecting the specificity of tripartite motif containing-21 scaffolds using a novel discovery and design approach. *J. Biol. Chem.* **2023**, *299* (12), 105381.

(10) Chan, A.; Haley, R. M.; Najar, M. A.; Gonzalez-Martinez, D.; Bugaj, L. J.; Burslem, G. M.; Mitchell, M. J.; Tsourkas, A. Lipid-mediated intracellular delivery of recombinant bioPROTACs for the rapid degradation of undruggable proteins. *Nat. Commun.* **2024**, *15* (1), 5808.

(11) Münick, P.; Zielinski, J.; Strubel, A.; Gutfreund, N.; Dreier, B.; Schaefer, J. V.; Schafer, B.; Gebel, J.; Osterburg, C.; Chaikuad, A.; et al. DARPins as a novel tool to detect and degrade p73. *Cell Death Dis.* **2024**, *15* (12), 909.

(12) Taylor, J. D.; Barrett, N.; Martinez Cuesta, S.; Cassidy, K.; Pachl, F.; Dodgson, J.; Patel, R.; Eriksson, T. M.; Riley, A.; Burrell, M.; et al. Targeted protein degradation using chimeric human E2 ubiquitin-conjugating enzymes. *Commun. Biol.* **2024**, *7* (1), 1179.

(13) Zhao, S.; Luo, J.; Xu, P.; Zeng, J.; Yan, G.; Yu, F.; Qin, L.; Zhang, C.; Li, P.; Cai, M.; et al. Designed peptide binders and nanobodies as PROTAC starting points for targeted degradation of PCNA and BCL6. *Int. J. Biol. Macromol.* **2025**, *308* (Pt 3), 142667.

(14) Jing, X.; Mackay, J. P.; Passioura, T. Macrocyclic peptides as a new class of targeted protein degraders. *RSC Chem. Biol.* **2025**, *6* (3), 326−337.

(15) Zhu, Y.; Dai, Y.; Tian, Y. The peptide PROTAC modality: a new strategy for drug discovery. *MedComm* **2025**, *6*, e70133.

(16) Lim, S.; Khoo, R.; Peh, K. M.; Teo, J.; Chang, S. C.; Ng, S.; Beilhartz, G. L.; Melnyk, R. A.; Johannes, C. W.; Brown, C. J.; et al. bioPROTACs as versatile modulators of intracellular therapeutic targets including proliferating cell nuclear antigen (PCNA). *Proc. Natl. Acad. Sci. U.S.A.* **2020**, *117* (11), 5791−5800.

(17) Hoffman, M.; Krum, D.; Wittrup, K. D. Bivalent target-binding bioPROTACs induce potent degradation of oncogenic SHP2. *J. Biol. Chem.* **2024**, *300* (9), 107616.

(18) Winkelvoß, D.; Vukovic, D.; Hanny, A. C.; Riermeier, L.; Udovcic, A.; Kolibius, J.; Honegger, A.; Mittl, P. R. E.; Michel, E.; Hansen, S.; et al. Molecular features defining the efficiency of bioPROTACs. *Commun. Biol.* **2025**, *8* (1), 946.

(19) Békés, M.; Langley, D. R.; Crews, C. M. PROTAC targeted protein degraders: the past is prologue. *Nat. Rev. Drug Discovery* **2022**, *21* (3), 181−200.

(20) Vukovic, D.; Winkelvoß, D.; Kapp, J.; Hänny, A.; Bürgisser, H.; Riermeier, L.; Udovcic, A.; Tiefenboeck, P.; Plückthun, A. Protein degradation kinetics measured by microinjection and live cell fluorescence microscopy. *Sci. Rep.* **2024**, *14*, 27153.

(21) Shin, Y. J.; Park, S. K.; Jung, Y. J.; Kim, Y. N.; Kim, K. S.; Park, O. K.; Kwon, S. H.; Jeon, S. H.; Trinh, L. A.; Fraser, S. E.; et al. Nanobody-targeted E3-ubiquitin ligase complex degrades nuclear proteins. *Sci. Rep.* **2015**, *5*, 14269.

(22) Brauchle, M.; Hansen, S.; Caussinus, E.; Lenard, A.; Ochoa-Espinosa, A.; Scholz, O.; Sprecher, S. G.; Plückthun, A.; Affolter, M. Protein interference applications in cellular and developmental biology using DARPins that recognize GFP and mCherry. *Biol. Open* **2014**, *3* (12), 1252−1261.

(23) Martinez-Fonts, K.; Davis, C.; Tomita, T.; Elsasser, S.; Nager, A. R.; Shi, Y.; Finley, D.; Matouschek, A. The proteasome 19S cap and its ubiquitin receptors provide a versatile recognition platform for substrates. *Nat. Commun.* **2020**, *11* (1), 477.

(24) Martinez-Fonts, K.; Matouschek, A. A rapid and versatile method for generating proteins with defined ubiquitin chains. *Biochemistry* **2016**, *55* (12), 1898−1908.

(25) Sakamoto, K. M.; Kim, K. B.; Kumagai, A.; Mercurio, F.; Crews, C. M.; Deshaies, R. J. Protacs: chimeric molecules that target proteins to the Skp1-Cullin-F box complex for ubiquitination and degradation. *Proc. Natl. Acad. Sci. U.S.A.* **2001**, *98* (15), 8554−8559.

(26) Sakamoto, K. M.; Kim, K. B.; Verma, R.; Ransick, A.; Stein, B.; Crews, C. M.; Deshaies, R. J. Development of PROTACs to target cancer-promoting proteins for ubiquitination and degradation. *Mol. Cell. Proteomics* **2003**, *2* (12), 1350−1358.

(27) Zhang, C.; Li, X.; Adelmant, G.; Dobbins, J.; Geisen, C.; Oser, M. G.; Wucherpfenning, K. W.; Marto, J. A.; Kaelin, W. G., Jr. Peptidic degron in EID1 is recognized by an SCF E3 ligase complex containing the orphan F-box protein FBXO21. *Proc. Natl. Acad. Sci. U.S.A.* **2015**, *112* (50), 15372−15377.

(28) D'Angiolella, V.; Donato, V.; Forrester, F. M.; Jeong, Y. T.; Pellacani, C.; Kudo, Y.; Saraf, A.; Florens, L.; Washburn, M. P.; Pagano, M. Cyclin F-mediated degradation of ribonucleotide reductase M2 controls genome integrity and DNA repair. *Cell* **2012**, *149* (5), 1023−1034.

(29) Zhang, D.; Baek, S. H.; Ho, A.; Kim, K. Degradation of target protein in living cells by small-molecule proteolysis inducer. *Bioorg. Med. Chem. Lett.* **2004**, *14* (3), 645−648.

(30) Montrose, K.; Krissansen, G. W. Design of a PROTAC that antagonizes and destroys the cancer-forming X-protein of the hepatitis B virus. *Biochem. Biophys. Res. Commun.* **2014**, *453* (4), 735−740.

(31) Gu, J.; Chen, D.; Rosenblum, J.; Rubin, R. M.; Yuan, Z. M. Identification of a sequence element from p53 that signals for Mdm2-targeted degradation. *Mol. Cell. Biol.* **2000**, *20* (4), 1243−1253.

(32) Melvin, A. T.; Woss, G. S.; Park, J. H.; Dumberger, L. D.; Waters, M. L.; Allbritton, N. L. A comparative analysis of the ubiquitination kinetics of multiple degrons to identify an ideal targeting sequence for a proteasome reporter. *PLoS One* **2013**, *8* (10), e78082.

(33) Melvin, A. T.; Dumberger, L. D.; Woss, G. S.; Waters, M. L.; Allbritton, N. L. Identification of a p53-based portable degron based on the MDM2-p53 binding region. *Analyst* **2016**, *141* (2), 570−578.

(34) Kuang, Z.; Lewis, R. S.; Curtis, J. M.; Zhan, Y.; Saunders, B. M.; Babon, J. J.; Kolesnik, T. B.; Low, A.; Masters, S. L.; Willson, T. A.; et al. The SPRY domain-containing SOCS box protein SPSB2 targets iNOS for proteasomal degradation. *J. Cell Biol.* **2010**, *190* (1), 129−141.

(35) Nishiya, T.; Matsumoto, K.; Maekawa, S.; Kajita, E.; Horinouchi, T.; Fujimuro, M.; Ogasawara, K.; Uehara, T.; Miwa, S. Regulation of inducible nitric-oxide synthase by the SPRY domain- and SOCS box-containing proteins. *J. Biol. Chem.* **2011**, *286* (11), 9009−9019.

(36) Bonger, K. M.; Chen, L. C.; Liu, C. W.; Wandless, T. J. Small-molecule displacement of a cryptic degron causes conditional protein degradation. *Nat. Chem. Biol.* **2011**, *7* (8), 531−537.
(37) Koren, I.; Timms, R. T.; Kula, T.; Xu, Q.; Li, M. Z.; Elledge, S. J. The eukaryotic proteome is shaped by E3 ubiquitin ligases targeting C-terminal degrons. *Cell* **2018**, *173* (7), 1622−1635.e14.
(38) Mercer, A. A.; Fleming, S. B.; Ueda, N. F-box-like domains are present in most poxvirus ankyrin repeat proteins. *Virus Genes* **2005**, *31* (2), 127−133.
(39) Sonnberg, S.; Seet, B. T.; Pawson, T.; Fleming, S. B.; Mercer, A. A. Poxvirus ankyrin repeat proteins are a unique class of F-box proteins that associate with cellular SCF1 ubiquitin ligase complexes. *Proc. Natl. Acad. Sci. U.S.A.* **2008**, *105* (31), 10955−10960.
(40) Werden, S. J.; Lanchbury, J.; Shattuck, D.; Neff, C.; Dufford, M.; McFadden, G. The myxoma virus M-T5 ankyrin repeat host range protein is a novel adaptor that coordinately links the cellular signaling pathways mediated by Akt and Skp1 in virus-infected cells. *J. Virol.* **2009**, *83* (23), 12068−12083.
(41) Sperling, K. M.; Schwantes, A.; Schnierle, B. S.; Sutter, G. The highly conserved orthopoxvirus 68k ankyrin-like protein is part of a cellular SCF ubiquitin ligase complex. *Virology* **2008**, *374* (2), 234−239.
(42) Lim, S.; Khoo, R.; Juang, Y. C.; Gopal, P.; Zhang, H.; Yeo, C.; Peh, K. M.; Teo, J.; Ng, S.; Henry, B.; et al. Exquisitely specific anti-KRAS biodegraders inform on the cellular prevalence of nucleotide-loaded states. *ACS Cent. Sci.* **2021**, *7* (2), 274−291.
(43) Hatakeyama, S.; Watanabe, M.; Fujii, Y.; Nakayama, K. I. Targeted destruction of c-Myc by an engineered ubiquitin ligase suppresses cell transformation and tumor formation. *Cancer Res.* **2005**, *65* (17), 7874−7879.
(44) Stephens, E. A.; Ludwicki, M. B.; Meksiriporn, B.; Li, M.; Ye, T.; Monticello, C.; Forsythe, K. J.; Kummer, L.; Zhou, P.; Plückthun, A.; et al. Engineering single pan-specific ubiquibodies for targeted degradation of all forms of endogenous ERK protein kinase. *ACS Synth. Biol.* **2021**, *10* (9), 2396−2408.
(45) Portnoff, A. D.; Stephens, E. A.; Varner, J. D.; DeLisa, M. P. Ubiquibodies, synthetic E3 ubiquitin ligases endowed with unnatural substrate specificity for targeted protein silencing. *J. Biol. Chem.* **2014**, *289* (11), 7844−7855.
(46) Ishigaki, S.; Niwa, J.; Yamada, S.; Takahashi, M.; Ito, T.; Sone, J.; Doyu, M.; Urano, F.; Sobue, G. Dorfin-CHIP chimeric proteins potently ubiquitylate and degrade familial ALS-related mutant SOD1 proteins and reduce their cellular toxicity. *Neurobiol. Dis.* **2007**, *25* (2), 331−341.
(47) Zhong, D.; Ru, Y.; Wang, Q.; Zhang, J.; Zhang, J.; Wei, J.; Wu, J.; Yao, L.; Li, X.; Li, X. Chimeric ubiquitin ligases inhibit non-small cell lung cancer via negative modulation of EGFR signaling. *Cancer Lett.* **2015**, *359* (1), 57−64.
(48) Wang, Q.; Ru, Y.; Zhong, D.; Zhang, J.; Yao, L.; Li, X. Engineered ubiquitin ligase PTB-U-box targets insulin/insulin-like growth factor receptor for degradation and coordinately inhibits cancer malignancy. *Oncotarget* **2014**, *5* (13), 4945−4958.
(49) Pan, T.; Zhang, Y.; Zhou, N.; He, X.; Chen, C.; Liang, L.; Duan, X.; Lin, Y.; Wu, K.; Zhang, H. A recombinant chimeric protein specifically induces mutant KRAS degradation and potently inhibits pancreatic tumor growth. *Oncotarget* **2016**, *7* (28), 44299−44309.
(50) Ma, Y.; Gu, Y.; Zhang, Q.; Han, Y.; Yu, S.; Lu, Z.; Chen, J. Targeted degradation of KRAS by an engineered ubiquitin ligase suppresses pancreatic cancer cell growth in vitro and in vivo. *Mol. Cancer Ther.* **2013**, *12* (3), 286−294.
(51) Bery, N.; Miller, A.; Rabbitts, T. A potent KRAS macromolecule degrader specifically targeting tumours with mutant KRAS. *Nat. Commun.* **2020**, *11* (1), 3233.
(52) Nordquist, K. A.; Dimitrova, Y. N.; Brzovic, P. S.; Ridenour, W. B.; Munro, K. A.; Soss, S. E.; Caprioli, R. M.; Klevit, R. E.; Chazin, W. J. Structural and functional characterization of the monomeric U-box domain from E4B. *Biochemistry* **2010**, *49* (2), 347−355.
(53) Ludwicki, M. B.; Li, J.; Stephens, E. A.; Roberts, R. W.; Koide, S.; Hammond, P. T.; DeLisa, M. P. Broad-spectrum proteome editing with an engineered bacterial ubiquitin ligase mimic. *ACS Cent. Sci.* **2019**, *5* (5), 852−866.
(54) Luo, Z.; Pan, Y.; Jeong, L. S.; Liu, J.; Jia, L. Inactivation of the Cullin (CUL)-RING E3 ligase by the NEDD8-activating enzyme inhibitor MLN4924 triggers protective autophagy in cancer cells. *Autophagy* **2012**, *8* (11), 1677−1679.
(55) Prakash, S.; Tian, L.; Ratliff, K. S.; Lehotzky, R. E.; Matouschek, A. An unstructured initiation site is required for efficient proteasome-mediated degradation. *Nat. Struct. Mol. Biol.* **2004**, *11* (9), 830−837.
(56) Herman, A. G.; Hayano, M.; Poyurovsky, M. V.; Shimada, K.; Skouta, R.; Prives, C.; Stockwell, B. R. Discovery of Mdm2-MdmX E3 ligase inhibitors using a cell-based ubiquitination assay. *Cancer Discovery* **2011**, *1* (4), 312−325.
(57) Ivan, M.; Kondo, K.; Yang, H.; Kim, W.; Valiando, J.; Ohh, M.; Salic, A.; Asara, J. M.; Lane, W. S.; Kaelin, W. G., Jr. HIFalpha targeted for VHL-mediated destruction by proline hydroxylation: implications for O2 sensing. *Science* **2001**, *292* (5516), 464−468.
(58) Becker, L.; Singh Badwal, J.; Brandl, F.; Verdurmen, W. P. R.; Plückthun, A. Thermodynamic stability Is a strong predictor for the delivery of DARPins to the cytosol via anthrax toxin. *Pharmaceutics* **2021**, *13* (8), 1285.
(59) Johnston, J. B.; Wang, G.; Barrett, J. W.; Nazarian, S. H.; Colwill, K.; Moran, M.; McFadden, G. Myxoma virus M-T5 protects infected cells from the stress of cell cycle arrest through its interaction with host cell cullin-1. *J. Virol.* **2005**, *79* (16), 10750−10763.
(60) Qian, S. B.; Waldron, L.; Choudhary, N.; Klevit, R. E.; Chazin, W. J.; Patterson, C. Engineering a ubiquitin ligase reveals conformational flexibility required for ubiquitin transfer. *J. Biol. Chem.* **2009**, *284* (39), 26797−26802.
(61) Zhuang, M.; Calabrese, M. F.; Liu, J.; Waddell, M. B.; Nourse, A.; Hammel, M.; Miller, D. J.; Walden, H.; Duda, D. M.; Seyedin, S. N.; et al. Structures of SPOP-substrate complexes: insights into molecular architectures of BTB-Cul3 ubiquitin ligases. *Mol. Cell* **2009**, *36* (1), 39−50.
(62) Park, S. W.; Lee, D. S.; Kim, Y. S. Engineering a U-box of E3 ligase E4B through yeast surface display-based functional screening generates a variant with enhanced ubiquitin ligase activity. *Biochem. Biophys. Res. Commun.* **2022**, *612*, 147−153.
(63) Galdeano, C.; Gadd, M. S.; Soares, P.; Scaffidi, S.; Van Molle, I.; Birced, I.; Hewitt, S.; Dias, D. M.; Ciulli, A. Structure-guided design and optimization of small molecules targeting the protein-protein interaction between the von Hippel-Lindau (VHL) E3 ubiquitin ligase and the hypoxia inducible factor (HIF) alpha subunit with in vitro nanomolar affinities. *J. Med. Chem.* **2014**, *57* (20), 8657−8663.
(64) Fischer, E. S.; Böhm, K.; Lydeard, J. R.; Yang, H.; Stadler, M. B.; Cavadini, S.; Nagel, J.; Serluca, F.; Acker, V.; Lingaraju, G. M.; et al. Structure of the DDB1-CRBN E3 ubiquitin ligase in complex with thalidomide. *Nature* **2014**, *512* (7512), 49−53.
(65) Ito, T.; Ando, H.; Suzuki, T.; Ogura, T.; Hotta, K.; Imamura, Y.; Yamaguchi, Y.; Handa, H. Identification of a primary target of thalidomide teratogenicity. *Science* **2010**, *327* (5971), 1345−1350.
(66) Cyrus, K.; Wehenkel, M.; Choi, E. Y.; Han, H. J.; Lee, H.; Swanson, H.; Kim, K. B. Impact of linker length on the activity of PROTACs. *Mol. Biosyst.* **2011**, *7* (2), 359−364.
(67) Wang, C.; Zhang, Y.; Chen, W.; Wu, Y.; Xing, D. New-generation advanced PROTACs as potential therapeutic agents in cancer therapy. *Mol. Cancer* **2024**, *23* (1), 110.
(68) Becker, L.; Plückthun, A. DARPins bind their cytosolic targets after having been translocated through the protective antigen pore of anthrax toxin. *Sci. Rep.* **2023**, *13* (1), 8048.
(69) Schmit, N. E.; Neopane, K.; Hantschel, O. Targeted protein degradation through cytosolic delivery of monobody binders using bacterial toxins. *ACS Chem. Biol.* **2019**, *14* (5), 916−924.
(70) Sung, Y. K.; Kim, S. Recent advances in the development of gene delivery systems. *Biomaterials Res.* **2019**, *23* (1), 8.
(71) Simon, M.; Zangemeister-Wittke, U.; Plückthun, A. Facile double-functionalization of designed ankyrin repeat proteins using

click and thiol chemistries. *Bioconjugate Chem.* **2012**, *23* (2), 279–286.
(72) Studier, F. W. Stable expression clones and auto-induction for protein production in E. coli. *Methods Mol. Biol.* **2014**, *1091*, 17–32.
(73) Tan, Y.; Ci, Y.; Dai, X.; Wu, F.; Guo, J.; Liu, D.; North, B. J.; Huo, J.; Zhang, J. Cullin 3SPOP ubiquitin E3 ligase promotes the poly-ubiquitination and degradation of HDAC6. *Oncotarget* **2017**, *8* (29), 47890–47901.

https://doi.org/10.1021/acschembio.5c00569
ACS Chem. Biol. XXXX, XXX, XXX–XXX